Hindawi
Shock and Vibration
Volume 2018, Article ID 3435249, 14 pages
https://doi.org/10.1155/2018/3435249

Research Article

Numerical and Experimental Modal Analysis Applied to an Optical Test System Designed for the Form Measurements of Metre-Scale Optics

P. G. Golanó,[1] L. Zanotti Fragonara,[2] P. Morantz,[1] and R. Jourdain[1]

[1]*Cranfield University, School of Aerospace, Transportation and Manufacturing, Precision Engineering Institute, College Road, Cranfield MK43 0AL, UK*
[2]*Cranfield University, School of Aerospace, Transportation and Manufacturing, Centre for Autonomous and Cyberphysical Systems, College Road, Cranfield MK43 0AL, UK*

Correspondence should be addressed to L. Zanotti Fragonara; l.zanottifragonara@cranfield.ac.uk

Received 1 March 2018; Revised 6 June 2018; Accepted 2 October 2018; Published 4 November 2018

Academic Editor: Matteo Aureli

The work focuses on the structural design and performances of a unique optical test system (OTS) used for measuring metre-scale optical surfaces. The investigation was carried out through a modal analysis. Two sets of results are presented. Both modal analysis of the entire OTS and transmissibility function related to its use as an optical system are carried out and analysed. The OTS is used for the measurements of the form accuracy at nanometre level of metre-scale concave surfaces. The OTS is a four and half-metre-tall mechanical structure made of bolted aluminium profiles, two structural platens, two dedicated precision positioning supports, a test piece, and a state-of-the-art laser interferometer. The OTS was numerically modelled and fully instrumented with triaxial accelerometers. The results of the modal analysis highlight the natural modes of the entire OTS. Both numerical and experimental methods are designed. The investigation methods are iterative. Indeed, a preliminary numerical model is created using finite element analysis (FEA). FEA results enable the determination of the dynamic range and suitable locations of accelerometers that are mounted onto the OTS for the experimental validation of the FEA model and further to carry out the transmissibility study. Natural frequencies, damping ratios, and mode shape values are obtained and scrutinized. These results are used for refining the FEA model. In fact, the lack of symmetry and the use of feet are identified as the key design feature that affects the OTS. The correlation between experimental and numerical results is within five percent for the first four modes. The results of the transmissibility study highlight the specific natural modes that influence the OTS measurement capability. Overall, the study enables to guide engineers and researchers towards a robust design using a validated and methodical approach.

1. Introduction

Among the various uncertainties that affect high-precision form measurements, vibrations can easily be the one with the most damaging effects. Typically, vibrations are considered when designing measurement systems and ultraprecision pieces of equipment. This issue has led the engineering community to define serviceability curves for the design of laboratory systems and equipment. They are referred as general vibration criteria [1]. The main issue with vibrations is that even a very low amplitude may be amplified and consequently degrade system performances. Besides common vibration sources such as other machinery operated in the nearby environment and background noise, the major concern is due to vibrations induced by human activities such as walking [2]. The typical frequency range to be monitored in laboratories and research facilities ranges between 1 Hz and 100 Hz [3].

In this paper, an optical test system (OTS) designed, fabricated, and characterised within the Precision Engineering Institute at Cranfield University was investigated to secure measurement repeatability and precision at nanometre level. The OTS was installed in a moderately challenging environment due to the remote location of the University. However, the environment was known to be affected by vibrations that arisen from services, machineries,

employee walks, and automobile circulation. The OTS was designed to be used for measurements of the form accuracy at nanometre level of metre-scale concave spherical surfaces. The radius of curvature of the test piece imposed a three-metre distance between the test piece and interferometer. The measurement technique used for this OTS is based on laser interferometry. This instrument provided a ~500 um spatial resolution of the measured topography. Other methods such as deflectometry [4, 5], Hartman test [6], or Sagnac interferometer [7] are available for large surfaces but they do not provide the same benefits. Whatever, all the optical measurement techniques are affected by both thermal and structural performances of the test system. This work focuses on the modal aspects of the authors' OTS.

Vibrations are transmitted to the OTS through either supports or acoustic pressure waves. The excitement of the natural frequencies of the OTS potentially deteriorates the measurement capability. The authors propose to use operational and experimental modal analysis [8] to estimate modal parameters from vibration data and using system identification theory applied on linear time-invariant system.

A preliminary numerical model (Section 2.2) was created using the finite element (FE) method. The FE results enabled the determination of the dynamic range and suitable locations of accelerometers that were mounted onto the OTS (Section 3.2) for the experimental validation and furthermore for carrying out the transmissibility study (Section 3.4).

The present study aims to assess, predict, and investigate the performance of this unique system within the framework of the optical measurements for providing a reference benchmark study.

2. The Optical Test System

2.1. The Description of the Optical Test System. The optical test system (OTS) under investigation was a unique system designed for the measurements of metre-scale specular surfaces. The OTS enabled the measurements of 3-metre spherical forms at nanometre level accuracy, using the laser interferometric technique. The OTS was also used for performing a variety of spectral analyses onto the topography obtained. The OTS design allowed to carry out both accurate and fast measurements. The OTS benefited of a low-cost mechanical design and a relatively small footprint in the laboratory. Another benefit was that it could potentially be adapted to a larger variety of test pieces.

The OTS was four and a half metres tall. The main structure was constituted by bolted aluminium extruded profiles. The profile square sections were 80 mm by 80 mm. The OTS supported a laser interferometer located at the top, a test piece, and a positioning support located at the bottom. These two distinct elements were mounted onto two aluminium platens that served different purposes. Indeed, the platens both ensured the structural integrity and enabled the precise positioning of the functional elements (Figure 1). Also, the OTS aluminium structure was supported by five insulating and levelling feet.

The upper platen of the OTS was equipped with a high-performance interferometer (ZYGO DynaFiz™) [9, 10]. The chosen interferometer technology led to a less demanding

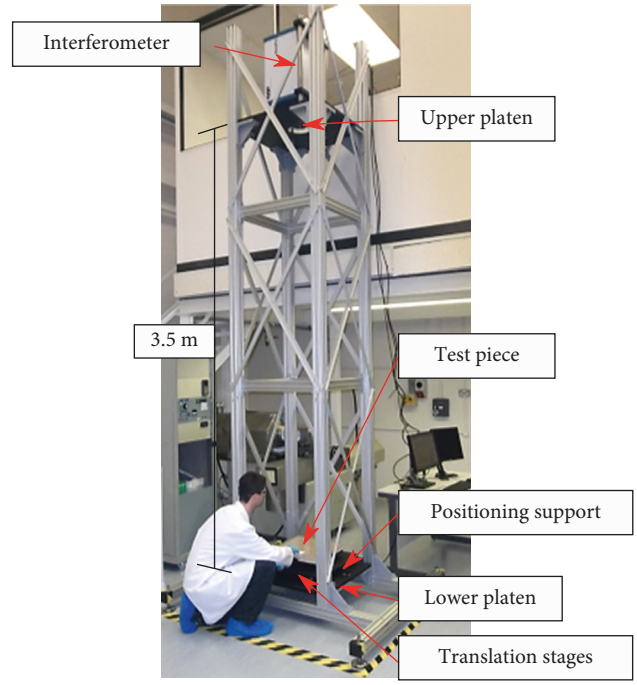

Figure 1: The OTS in the Precision Engineering Institute laboratory.

management of air turbulences [11, 12] because acquisition time was 12 microsecond and the data set obtained through a high number of acquisitions could be mathematically processed to remove the wavefront aberration due to structured and random air motions. On the other hand, the interferometer was significantly heavier compared to other instruments that also utilise interferometric techniques. Finally, the interferometer was held in a vertical manner by a specially designed support that was itself clamped onto the upper platen.

The lower platen supported both the test piece and its bespoke positioning support. The support allowed the fine positioning of the test piece surface through the adjustment of five degrees of freedom (three translations and two rotations). The test piece was placed on top of a 5 mm thick PVC open cell foam [13, 14] that enabled the surface-contact load to be uniformly distributed between the test piece and positioning support. After the foam had settled, the test piece was accurately positioned in the horizontal plan using two manual translation stages. Finally, three precision screws were used for the tip tilt adjustment. All these elements were critical and necessary from a functional viewpoint.

2.2. The Numerical Modelling of the OTS. A finite element (FE) model of the OTS was created using ANSYS (version 16.2). The block Lanczos algorithm was used for solving the eigenvalue system [15]. Also, the software package was used for the interpretation of the vibrational modes of the experimental modal analysis (i.e., model-based decision process [16]). In order to numerically model the OTS, one assumption was made, and initial conditions were set. Hereafter, both the detailed explanations and modelling approach are detailed.

First, the OTS was assumed to have linear behaviour. That assumption was justified because the amplitudes of the

vibrations were small. Indeed, the main source of excitations was the background noise of the University laboratory.

Second, the aluminium profiles of the mechanical structure were modelled by means of unidimensional beams. Element BEAM188 available in ANSYS library was used. The beams were meshed with an average element size of 40 mm that was determined through a mesh independency study not detailed in this paper. Whatever, Figure 2(a) shows the complete FE model. The model was composed of 2918 nodes and 2873 elements. Figure 2(b) shows the CAD model done using Siemens NX software.

Third, the bolted connections that constrained completely the motion of the parts were modelled using a rigid joint approach.

The upper and lower aluminium platens of the OTS were modelled using element SHELL181. The weight of each platen was implemented through this element too. Each platen weighted 32 kg.

Fourth, in the upper section of the OTS, the total mass of both the interferometer and the interferometer support structure (ISS) weighted 70 kg. The interferometer was modelled using lumped mass element named MASS21. The mass element was positioned using the centre of gravity (CoG) of the interferometer. On the other hand, the ISS was modelled using the BEAM188 elements. The ISS was made of two materials. The horizontal and the vertical parts were made of stainless steel and aluminium, respectively. The command CERIG was used for generating constrain equations also named rigid links (RL). The RLs were used between the selected six nodes of the ISS and the lump mass element (i.e., CoG of the interferometer). In addition, RLs were used for securing the transmission of inertia forces between the ISS and the upper platen. The numerical approach enabled the modelling of the mass asymmetry. Figure 3 shows the complete FE model of the OTS upper section.

Fifth, the lower platen held both the test piece support that weighted 16.6 kg and the test piece that weighted 15.6 kg. The test piece was made of ULE glass [17], and the dimensions were 420 mm × 420 mm × 40 mm. Figure 4(a) shows the complete FE model of the OTS lower section. Figure 4(b) shows the CAD model. It is clear that a high degree of simplification was implemented.

Sixth, the feet of the OTS were modelled using numerical artefacts equivalent to a set of three orthogonal linear springs. Element type COMBIN14 was chosen [15]. The OTS was supported by five antivibration polyamide feet that were bolted through the lower horizontal aluminium profiles (Figure 5). In practice, three feet were used as the main kinematic mount [18]. This design feature ensured the stability and the vertical adjustment of the OTS. The additional two feet were used for safety purposes and avoiding any rocking motions. In the FE model, all feet have the same numerical constrain. Figure 5 illustrates the modelled feet.

3. Experimental Modal Analysis

3.1. OTS Instrumentation. The equipment used for carrying out the experimental investigation and validate the FE model described in Section 2.2 is detailed hereafter. A LMS SCADAS III was used for multichannel dynamic data acquisition. It was used with both a set of four triaxial accelerometers (ICP® PCB Piezotronics models 2x 356A25 and 2x 356A25) and an impulse force test hammer (ICP® PCI Piezotronics model 086D20) using the super-soft tip in order to excite frequencies in the range 0–500 Hz. The system identification software used was LMS test lab.

The OTS structure was tested using the techniques of experimental and operational modal analysis (EMA and OMA, respectively) presented in [8, 19]. The next paragraph provides further details. The main difference between the two techniques is that in EMA, the input is directly measured whilst in OMA, only some assumptions about it can be done (e.g., input is white Gaussian noise [20]). OMA was firstly introduced in the area of civil engineering modal testing [8], where the input excitation to a structure is difficult or impractical to measure [21, 22].

For what concerns the experimental investigation, a complete inspection of the structure was conducted to ensure that all the two hundred screws were tightly screwed in up to the recommended torque. Also, the five feet were checked to ensure that they carried out adequate loading. This task secured an optimal and standardized experimental conditions.

The experimental tests were designed taking into account the first set of results of the FE model. Based on these preliminary results, it was possible to determine the sensor locations, the excitation locations, and the frequency bandwidth.

For what concerned the sensor locations procedure, a heuristic approach was chosen. Indeed, due to the relative simple mechanical design of the OTS, a coarse strategy was assessed to be sufficient [23] by the authors. Thus, the upper platen was chosen as the main excitation location. The platen was struck with the impulse test hammer. Two orthogonal directions were chosen. Directions X and Y and excitation locations are shown in Figure 6.

In total, 24 sensor locations were determined and used. The 24 locations provided 72 responses as triaxial accelerometers were used. The sensors were mainly mounted onto the four vertical aluminium extruded profiles along the different levels of the OTS (Figure 6 green dots). LMS Test.Lab software was used for signal acquisition and for system identification. The geometry of the OTS was defined within the acquisition software. Figure 6 shows the conceptual structure, excitation locations, and the locations of the sensors.

The entire OTS structure was investigated by changing the position of the sensors after each data acquisition (Figure 7). In practice, one sensor was set at a fixed position, and the other sensors were moved to fresh locations. The data of five impacts were averaged for each configuration.

All the acquisitions were made at a sampling frequency of the ADC of 360 Hz. The sampling was above the required Nyquist frequency for the frequency range in study up to 100 Hz. For this sampling frequency, the acquisition system used provided a minimum resolution of 0.15 Hz.

3.2. System Identification and Test Results. The system identification procedure was carried out after data cleaning, preprocessing and detrending using the default parameters

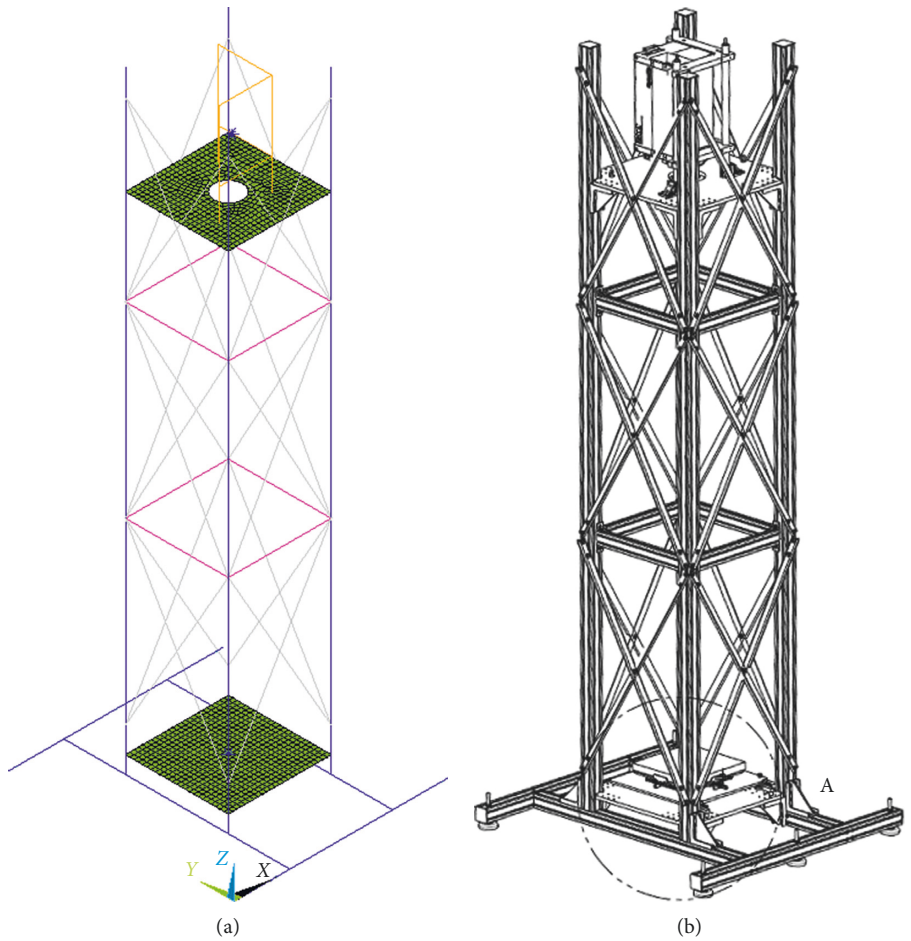

Figure 2: FEA model of the OTS (a) and CAD model (b).

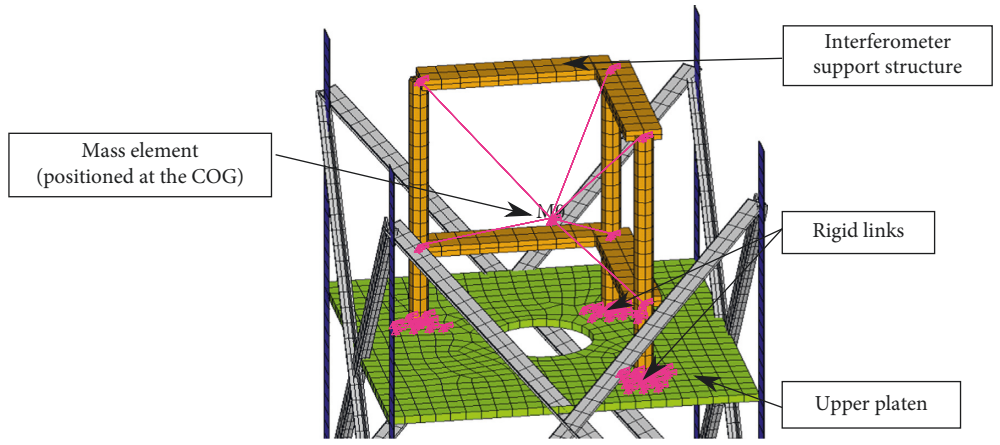

Figure 3: Upper platen and the interferometer support structure (ISS). In pink, rigid links can be seen.

of LMS Test.Lab (i.e., mean removal and low-pass filter at 200 Hz). The system identification of the modal parameters was carried out using PolyMAX software that solved the problem through a polyreference least-squares complex frequency (LSCF) domain method [24]. The LSCF based method allowed the extraction of natural frequencies, damping, and modal shapes. The method enabled the estimation of aforementioned values, where a common-denominator transfer function model was estimated with very small computational effort. This type of algorithm was used for obtaining a clear stabilisation chart (Figure 8). In the LSCF version of the algorithm, only eigenfrequencies and damping related to the pole information of the model can be extracted. Thus, the main drawback of this method is

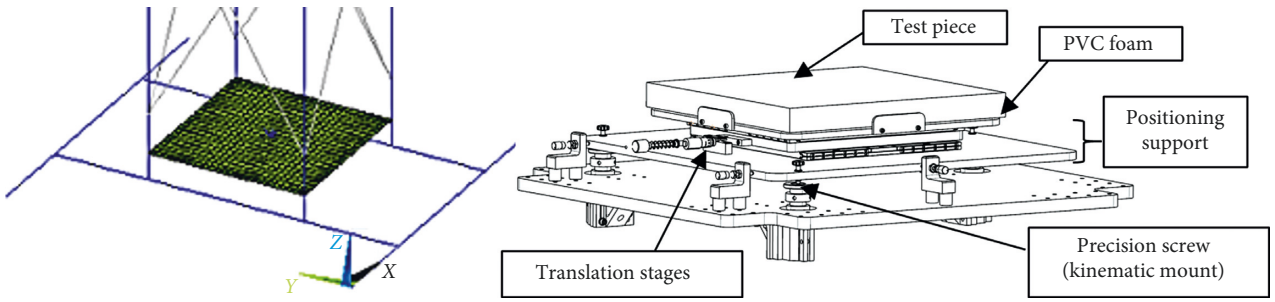

Figure 4: FEA model of the lower platen model (a) and CAD model (b).

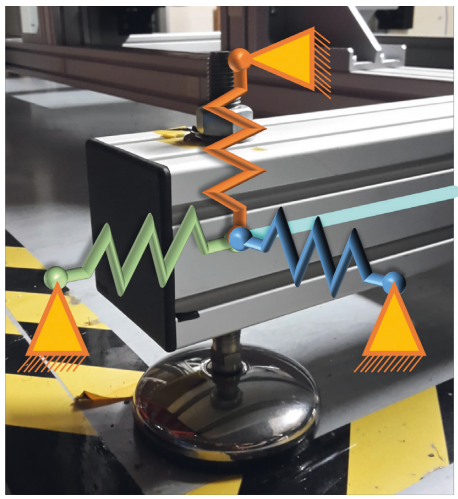

Figure 5: Levelling foot that supported the OTS. Superimposed, its modelling approach (three linear springs).

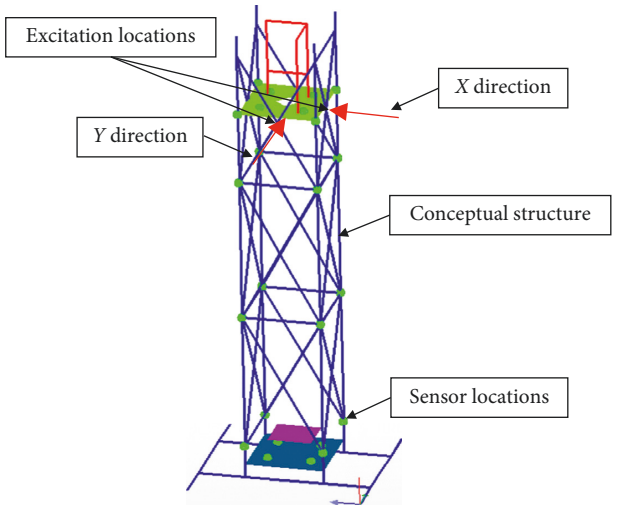

Figure 6: Excitation locations (green dots) and impact directions (red arrows) on the LMS Test.Lab geometry definition.

that participation factors or modal shapes cannot be directly estimated. PolyMAX, which is a polyreference version of the LSCF method, resorts to a right matrix-fraction model. In this study, also the participation factors are available in the construction of the stabilisation diagram. It has also better performance in decoupling closely spaced modes.

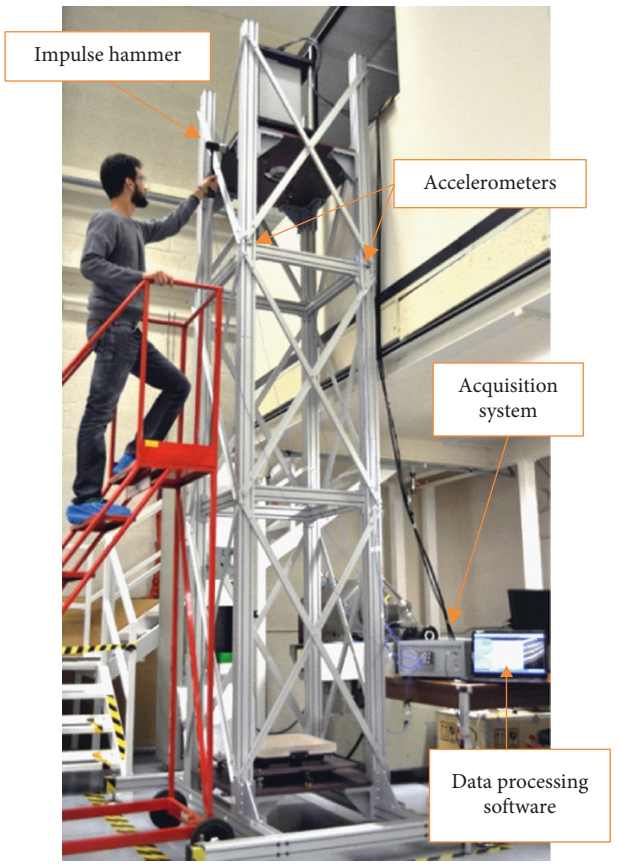

Figure 7: Experimental setup with equipment identified.

The main step of the identification process with LMS Test.Lab is the stabilisation chart for the bandwidth between 0 and 100 Hz and for a model order in the range 75–100. This chart is obtained when applying the LSCF method on the experimentally gathered information as a FRF function (Figure 8).

Only the clearly identified modes were selected in the 40–50 Hz bandwidth. The choice was also supported by the results of the numerical modal analysis. In fact, in this frequency range, the FE model helped to understand that many local bending modes of the various truss elements were grouped. Since local bending modes are not relevant to the measurements of the OTS, they were not used further in the analysis. From the point of view of experimental modal analysis (EMA), local vibrational modes (LVM)

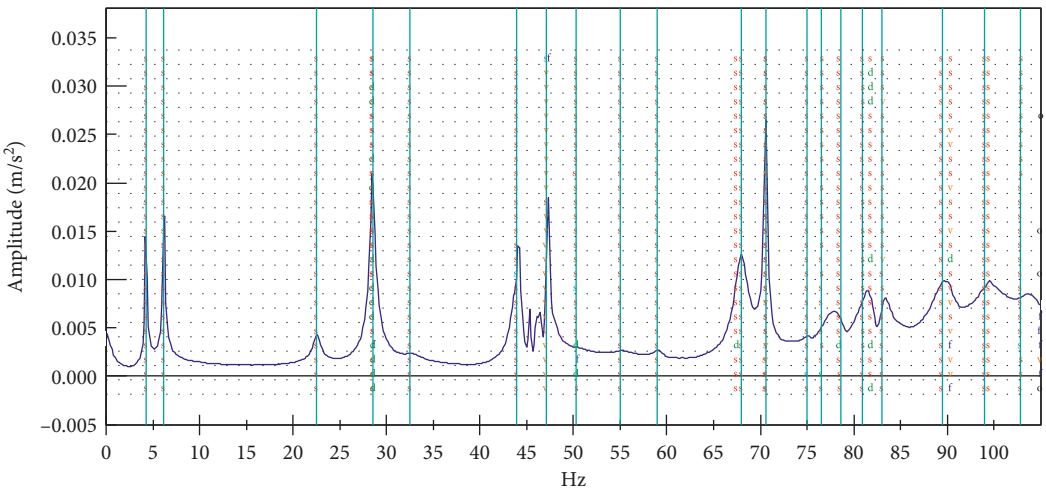

Figure 8: Stabilisation diagram for PolyMAX method (polyreference LSCF). Poles identified with an "S" represents a stabilisation in frequency, damping, and eigenvector. The blue solid line as the averaged sum of FRFs.

were less important because of the three reasons mentioned hereafter:

(1) LVM involved small fraction of mass in their vibration (thus the "local" name)

(2) LVM did not interfere with the global behaviour of the structure

(3) LVM did not strongly affect the quality of the measurements unless any global modes were coupled in the same area

The modal assurance criterion (MAC) was used as a quality assessment tool to check that the modes selected were independent and well defined. MAC is an indicator originally introduced to determine the quality of the experimental modal vectors [25]. It is a widely-accepted criterion for comparing modal shapes. The function of the MAC is to provide the correlation (not the orthogonality) between two different modal shapes and is comprised between 0 and 1.

At this point, the experimental modal parameters (i.e., frequencies, damping, and mode shapes) were obtained. The graphical visualization and the MAC criterion assisted in the pairing between the FE model and the EMA and also in the identification of discrepancy sources between the model and the real structure. For instance, mode 11 revealed an anomaly in the FE model with respect to the experimental results. This mode, identified at a frequency of 70.55 Hz, exhibited a deformation of the square storeys of the OTS. The modal shape is shown in Figure 9. Moreover, this mode showed a large amplitude on the average response function of the stabilisation diagram (Figure 8). This mode did not appear in the results of the FE model mainly because the internal joints of the structure square storeys were assumed infinitely rigid.

3.3. FE Model Updating and Matching. In order to validate the FE model, a comparison with the experimental results has been performed using the MAC between experimental and numerical mode shapes. The MAC values of the uncalibrated model are listed in Table 1.

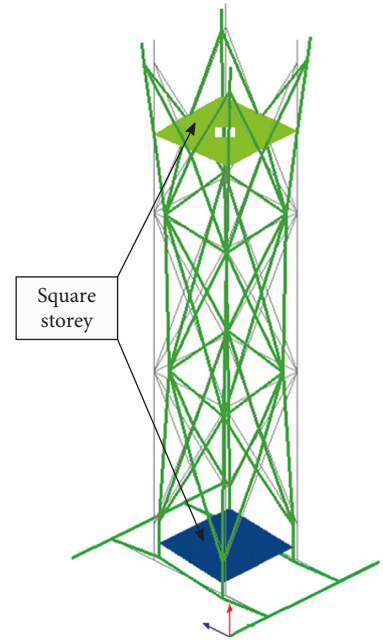

Figure 9: Mode shape at 70.6 Hz, mode 11 of the measured set (note: angular distortion of the square storeys of the OTS).

A model updating strategy was defined using an ad hoc MATLAB routine and a genetic algorithm minimising the penalty function:

$$\varepsilon(\mathbf{p}) = \sum_{i=1}^{m}\left[\alpha_i\left|\frac{\omega_{\mathrm{EMA},i} - \omega_{\mathrm{FEM},i}}{\omega_{\mathrm{EMA},i}}\right| + \beta_i\left(1 - \mathrm{MAC}_i\right)\right]. \quad (1)$$

The penalty function is defined as the normalised difference between the experimental and numerical eigenvalues ($\omega_{\mathrm{EMA},i}$ and $\omega_{\mathrm{FEM},i}$, respectively) and one minus the MAC value for the paired mode i. The vector $\mathbf{p}$ defines the dependency of the penalty function to the updating parameters (typically material properties in the FE model). The penalty

Table 1: Frequency and MAC discrepancies between the numerical and the experimental models before and after the model updating procedure.

Mode n°	EMA freq (Hz)	FEM freq (Hz)	FEM_{UPD} freq (Hz)	FEM error (%)	FEM_{UPD} error (%)	MAC	MAC_{UPD}
1	4.26	4.37	4.26	−2.51	0.00	0.99	0.98
2	6.18	6.42	6.36	−3.88	−2.91	0.99	0.97
3	22.52	22.05	22.52	2.09	0.00	0.94	0.94
4	28.50	30.07	30.01	−5.51	−5.30	0.47	0.47
5	32.49	38.18	33.42	−17.51	−2.86	0.47	0.51
6	43.91	46.08	44.95	−4.94	−2.37	0.56	0.55
7	55.01	57.15	51.82	−3.89	5.80	0.51	0.45
8	58.97	71.91	45.34	−21.94	23.11	0.46	0.42
9	67.90	83.34	64.78	−22.74	4.59	0.12	0.47
10	70.56	97.07	94.51	−37.57	−33.94	0.83	0.84

function (1) is generically used to update a FE model by using the diagonal values of the MAC matrix, computed between the experimental and numerical mode shapes. In this case, it has been chosen to consider also off-diagonal positions, in the case some modes are off-diagonal (wrong order in the FE model with respect to the experiments) or missing (local bending modes of the trusses are not identified via EMA, thus several local modes in the FE model have no correspondence in the experimental results). The modal pairing (or correlation) can be done accordingly to different methodologies (see Allemang [25] for a review). In this paper, it has been done using the same penalty function evaluated for each combination of modes and then paired using the minimum of each row in the experimental results. This procedure has several advantages: it is robust, it does not penalise excessively the updating procedures when modes are swapped but close in frequency, it is automatic (no need for manual pairing of modes), and it considers frequencies and not only mode shapes for pairing—opposite to a full MAC pairing procedure. A first graphical pairing between EMA and FE model is shown in Figure 10.

In the second step, the FE and experimental results were correlated resorting to the frequency and the mode shape assessments. At higher frequencies, the mode shapes were more complex and a direct graphical pairing was not possible. Whatever, it was acceptable to pair the modes in terms of frequency.

The error on the frequency and MAC values is shown in Table 1. This method guarantees the correct mode pairing up to the tenth mode and provides a quantitative evaluation of the performance of the models.

The model updating procedure has been carried out minimising the penalty function via a genetic algorithm (using the MATLAB optimisation toolbox) with an initial population size of 1000 samples and 30 iterations. The FE model has been interfaced directly with MATLAB to run the optimisation procedure sequentially, and the penalty function has been computed using the first 10 modes. It has been chosen to optimise the model resorting to 7 parameters.

The results of the model updating procedure are shown in Table 1. It is possible to notice how the frequency error reduces significantly. Before updating, 4 modes significantly differed in terms of frequency: mode 5, 8, 9, and mode 10. For what concerns MAC value, only one mode (number 9) was having a very low MAC, which meant that the first version (manually updated and refined) of the FE model was already a relatively good approximation of the structure. After the model updating procedure, frequency error decreased significantly, for 6 of the modes. In the case of mode 8 and 10, the updating did not lead to a significant improvement in frequency and MAC terms. In all other cases, the updating decreased either the frequency error or increased the MAC value. Typically, the frequency error of a model updating procedure is below 10% [26–28]. In this case, this is true for the first 7 modes of the structure. Consequently, the FE model was considered as successfully calibrated after the updating procedure.

3.4. Transmissibility Study. A transmissibility study was conducted to identify the transfer of mechanical vibrations throughout the structure in the operational conditions e.g., regular measurement. In fact, the results obtained through the modal analysis were not specific enough to highlight which of the identified modes may have adverse effects on the measurement capability of the OTS. Therefore, an experimental study of the system transmissibility was carried out.

Two points of interest were identified onto the OTS for computing the transmissibility function. The two points were named A and B (Figure 11). Both the reference lenses of the interferometer (Point B) and the test piece surface (Point A) were the appropriate locations for mounting the two accelerometers. But in practice, the mounting of an upper accelerometer onto the reference lens would have ruined the reference lens. Then the upper accelerometer was mounted onto the mount of the reference lens as shown in Figure 12(b). Whatever, the measurements were unlikely to be strongly affected.

3.4.1. Theory of Transmissibility Function. The motion transmissibility function [29] is defined as the ratio T that indicates the relative vibration levels between two points (j, k):

$$T_{jk}(\omega) = \frac{X_j \cdot e^{i\omega t}}{X_k \cdot e^{i\omega t}}. \quad (2)$$

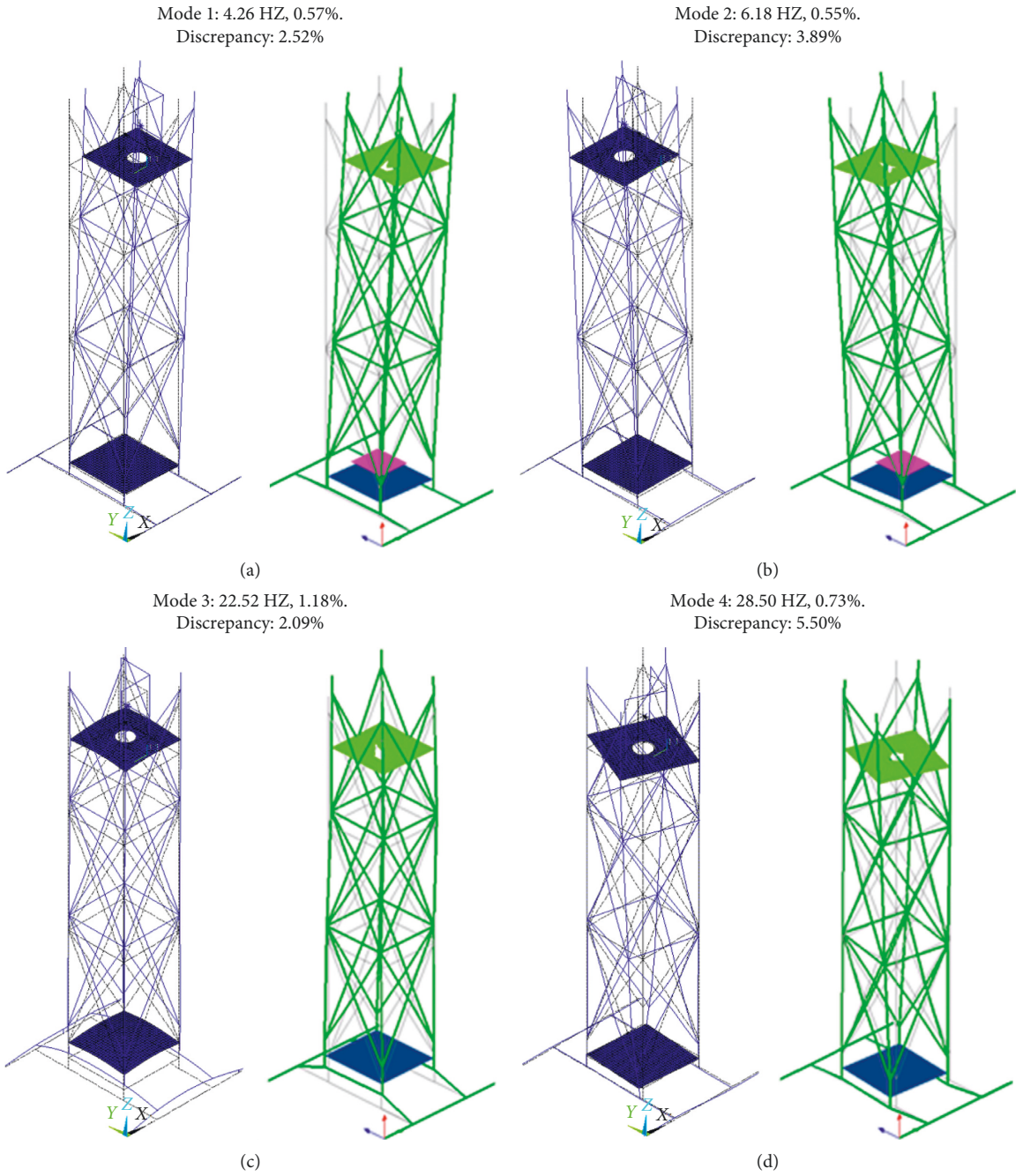

Figure 10: The first 4 paired modes. Frequency, damping, and discrepancy between the model (a, c) and the experimental results (b, d).

Transmissibility T can be determined, as the ratio between two transfer functions H with a common excitation point (i):

$$iT_{jk}(\omega) = \frac{H_{ji}(\omega)}{H_{ki}(\omega)}. \tag{3}$$

Normally, transmissibility T depends on the excitation point (i) or (q):

$$iT_{jk}(\omega) \neq qT_{jk}(\omega). \tag{4}$$

Nevertheless, near the resonance frequencies ω_r, the ratio becomes independent of the excitation point:

$$iT_{jk}(\omega) = \frac{H_{ji}(\omega)}{H_{ki}(\omega)} = \frac{\sum_r \left(\left(\phi_{jr}\phi_{ir}\right)/\left(\omega_r^2 - \omega^2\right)\right)}{\sum_r \left(\left(\phi_{kr}\phi_{ir}\right)/\left(\omega_r^2 - \omega^2\right)\right)}, \tag{5}$$

$$iT_{jk}(\omega)_{\omega \longrightarrow \omega_r} = \frac{\phi_{jr}}{\phi_{kr}}. \tag{6}$$

The motion transmissibility function is particularly useful when investigating vibration isolation systems and when the structure is lightly damped and that only one mode dominates the response near resonance [30, 31]. This is the case for the global vibration modes of the OTS (i.e., no coupled modes).

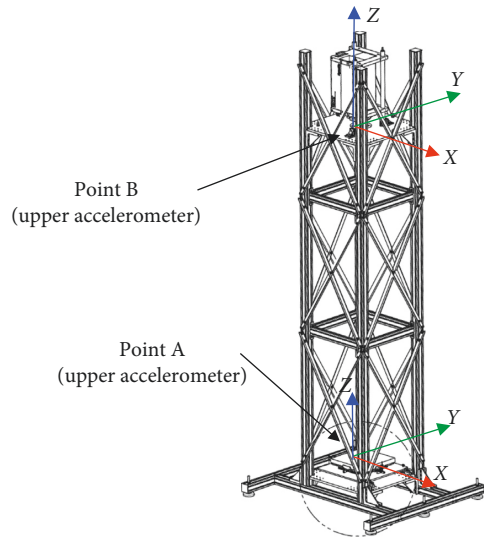

Figure 11: OTS and the two sets of Cartesian coordinate systems used for computing transmissibility functions.

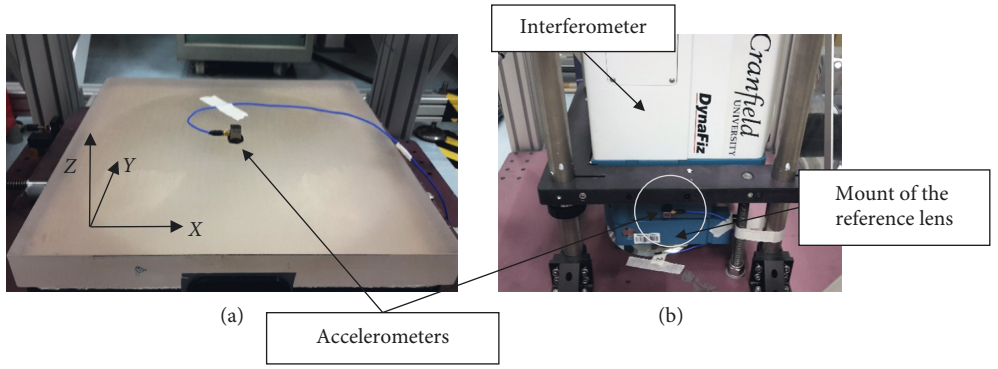

Figure 12: (a) The accelerometer on the test piece centre. (b) The accelerometer secured onto the mount of the reference lens.

3.4.2. Experimental Setup. The experimental setup for the measurement of the transmissibility function was carried out using two accelerometers. One accelerometer was positioned on the centre of the test piece (Figure 12(a)) and the other one was secured on the mount of the reference lens of the interferometer (Figure 12(b)). Their axes (X, Y, and Z) were parallel between them to compute later the transmissibility functions in the three different directions.

3.4.3. Results and Discussion. The transmissibility function in a structure as the one under investigation is independent from the point of excitation (Equation (6)). Nevertheless, in practice, slightly different transmissibility functions were obtained when changing the excitation position. This is very much influenced by the test type, using IHT, where only specific frequency bands can be excited depending on the head type. The transmissibility functions have been computed using offline postprocessing of the data with autopower and crosspower as input. To reduce that variability, the transmissibility function was computed by averaging the results obtained through different excitation locations, but using only parallel excitation directions. Figure 13 shows the transmissibility ratios computed between the mount of the reference lens (i.e., upper accelerometer) and the test piece (i.e., lower accelerometer). The ratios are expressed in dB, with respect to the frequency bandwidth 0 up to 100 Hz. The grey lines overlapped to the graph correspond to the mode frequencies identified through the EMA.

Transmissibility starts at 0 Hz in the X and Y direction with a value close to 0 dB. This is probably due to the type of excitation used (impact hammer test) which is not reliable for low frequencies and therefore transmissibility ratio tends to 0 dB. More reliable values of the X and Y transmissibility start near the first mode until a broad peak at 20 Hz. These two transmissibility functions were characteristic of the motions measured in the horizontal plan (X-Y directions). This result highlights the presences and effects of the two main dominating modes. These modes identified at 4.3 and 6.2 Hz are the first two bending modes in the X and Y direction, respectively. They caused a relative displacement of the upper end of the OTS. They were characterised by larger vibrational amplitudes of the upper part of the OTS. The 1st and 2nd bending modes are displayed in Figure 10 (top). The lower part of the tower was almost static, which explains the high values on the transmissibility function on the test piece

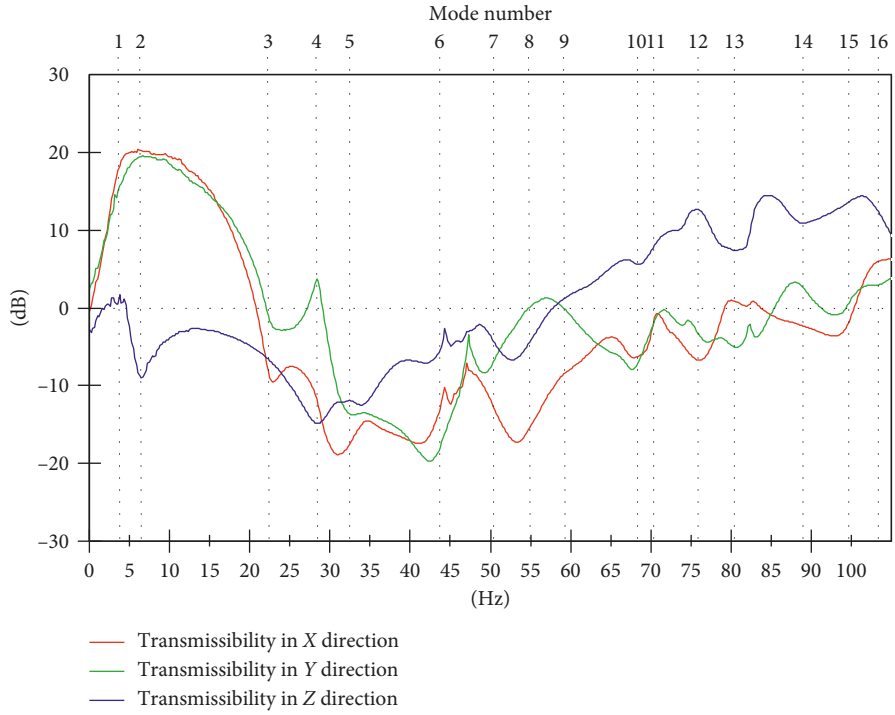

Figure 13: Transmissibility ratios in X, Y, and Z directions between the accelerometer placed in the test piece and the one mounted on the reference lens. The ratios are averaged between different excitation locations.

horizontal plane. These modes dominated the dynamic response because they were the easiest modes to excite.

The fourth mode, named torsional mode (Figure 10(d)), enabled the highlighting of a potential effect of the structural design on the measurement. Indeed by 28.5 Hz, both X and Y direction transmissibility functions increase again.

The differences between X and Y directions could be explained by the nonperfect positioning of the accelerometers. Indeed, as mentioned in Section 3.4 paragraph 2, the upper accelerometer was not positioned onto the main optical axis of the test system. But more importantly, it must be emphasised that the OTS structure is asymmetric. The effects are evident for mode 4, which is a torsional mode, where one would expect similar values of the transmissibility function. In any case, the effects of the interferometer supporting structure affect the overall global torsional behaviour, having a local bending of the structure in the Y-direction. These remarks and observations can be extrapolated on the other frequencies.

The transmissibility function in the Z (vertical) direction tends to increase for frequencies above 50 Hz. No direct explanations could be found. In any case, the mode shapes for these high frequencies become more complex and not easily distinguishable even with a relatively dense setup.

At this point, it is important to mention that the test piece both was supported by a complex positioning support (Figure 4(b)) and rested on polyvinyl chloride (PVC) open cell foam. Also, the interferometer was secured on the upper platen by the ISS (Figure 3) that was designed for providing three degrees of freedom: two rotations and one translation. These two dedicated supports introduce complexity in the dynamic of the system. Therefore, a second transmissibility function was computed between the upper and lower aluminium platens in order to be able to determine the transmissibility "to" and "through" the lower plate and the support system.

Figures 14 and 15 show the results obtained in X and Y directions, respectively. Results enable a direct comparison between the current and previous set of results. The transmissibility functions between interferometer and test piece (green plot) show both lower amplitudes and a relatively similar function shape. The transmissibility function shows the efficacy of the 5 mm PVC foam that was positioned between the test piece and the aluminium plate. The PVC foam insulates the test piece from vibrations throughout the whole bandwidth, except in the range 80–100 Hz. Whatever, the authors could not exclude the effect of the ISS.

As a matter of comparison, the transmissibility functions between the lower and upper platen computed with the updated FE model are reported in Figures 16 and 17 for the X and Y direction (in order to save space, the Z-direction, less relevant, is omitted). It is possible to notice how the large amplification area between 0 and 25 Hz, in the range of 20 dB is present in the model as well. The transmissibility differs in the central area (besides some peak shifting, due to the not perfect tuning of the model), as several sharp peaks are present, whilst in the experimental transmissibilities, everything is smoothed. This is certainly due to: the not optimal excitation used for the computation of the transmissibilities (impact hammer), the averaging procedure (the FE model results are not averaged), and the experimental noise.

In the Z direction (Figure 18), the graph lines are less similar. Below 60 Hz, the transmissibility function of the

Figure 14: Comparison of the two transmissibility functions in X direction.

Figure 15: Comparison of the two transmissibility functions in Y direction.

OTS remained below the transmissibility function of the platens. The amplitude increases above that frequency. The main hypothesis to explain the increase in amplitude is the appearance of local modes in the ISS or in the test piece support.

4. Conclusions

This paper presented both the experimental and numerical methods to determine the modal characteristics of a metre-scale optical test system (OTS). A finite element model of the OTS was created and a modal analysis was performed. On the other hand, an experimental modal analysis was carried out. The correlation between the experimental and finite element approaches was improved resorting to a model updating procedure. A maximum 5% discrepancy on the natural frequencies was achieved for a frequency range between 0 and 30 Hz. Then, a transmissibility study was carried out between the key optical components: the interferometer and the test piece. This transmissibility study highlighted the dynamic response of the OTS and the effect it may have on its performance. The results revealed the effects of some particular vibration modes on the measurement capability. It was determined that the first two modes (4.26 Hz and 6.18 Hz) are

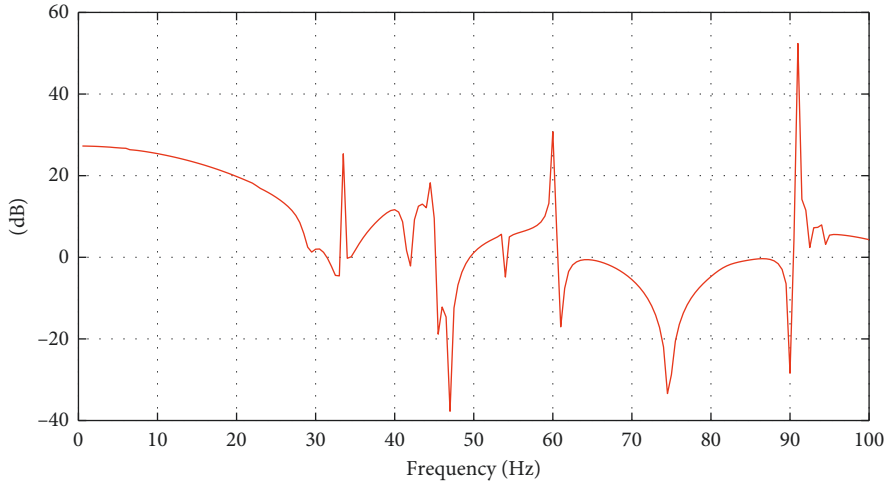

Figure 16: FEM Transmissibility between lower and upper platen.

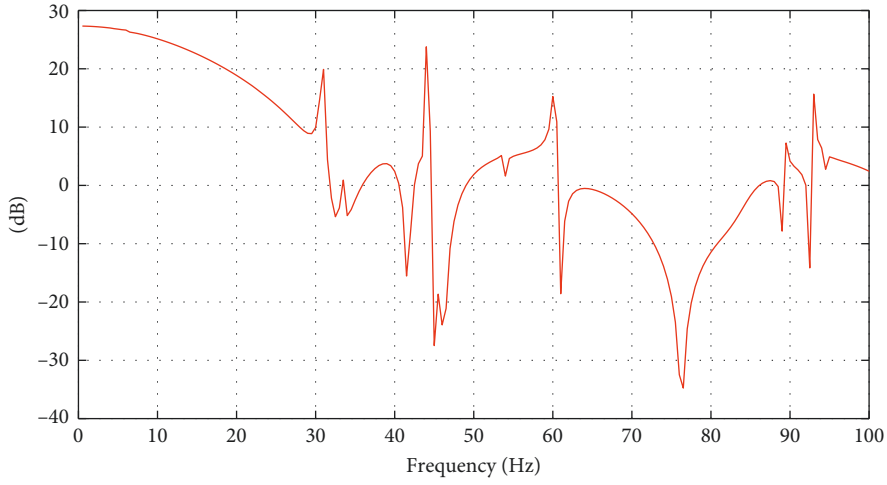

Figure 17: FEM Transmissibility in Y-direction between lower and upper platen.

Figure 18: Comparison of the two transmissibility functions in Z direction.

likely to present the most detrimental effects. The study set the foundations for a further investigation on interferometer-based measurement systems.

Acronyms

ADC: Analog-to-digital converter
CAD: Computer-aided design
EMA: Experimental modal analysis
FE: Finite element
FEA: Finite element analysis
ISS: Interferometer structure support
LSCF: Least-squares complex frequency
LVM: Local vibrational modes
MAC: Modal assurance criterion
OTS: Optical test system
PVC: Polyvinyl chloride
RL: Rigid link
ULE: Ultra-low expansion.

Data Availability

The data used to support the findings of this study are available from the corresponding author upon request.

Conflicts of Interest

The authors declare that there are no conflicts of interest regarding the publication of this paper.

References

[1] C. G. Gordon, "Generic criteria for vibration-sensitive equipment," in *Proceedings of Vibration Control in Microelectronics, Optics, and Metrology*, vol. 1619, pp. 71–85, San Jose, CA, USA, 1992.

[2] T.-C. Pan, X. You, and C. L. Lim, "Evaluation of floor vibration in a biotechnology laboratory caused by human walking," *Journal of Performance of Constructed Facilities*, vol. 22, no. 3, pp. 122–130, 2008.

[3] B. Bessason, C. Madshus, H. A. Frøystein, and H. Kolbjørnsen, "Vibration criteria for metrology laboratories," *Measurement Science and Technology*, vol. 10, no. 11, pp. 1009–1014, 1999.

[4] M. Xiao, T. Takamura, S. Takahashi, and K. Takamasu, "Random error analysis of profile measurement of large aspheric optical surface using scanning deflectometry with rotation stage," *Precision Engineering*, vol. 37, no. 3, pp. 599–605, 2013.

[5] E. Hofbauer and R. Rascher, "Deflectometric acquisition of large optical surfaces DaOS," *Optik & Photonik*, vol. 11, no. 5, pp. 40–44, 2016.

[6] P. Su, M. A. H. Khreishi, T. Su et al., "Aspheric and freeform surfaces metrology with software configurable optical test system: a computerized reverse Hartmann test," *Optical Engineering*, vol. 53, no. 3, article 31305, 2013.

[7] S. Chatterjee and Y. Pavan Kumar, "Determination of the surface form error of a spherical mirror with phase shifting Sagnac interferometer," *Applied Optics*, vol. 53, no. 14, p. 3069, 2014.

[8] E. Reynders, "System identification methods for (operational) modal analysis: review and comparison," *Archives of Computational Methods in Engineering*, vol. 19, no. 1, pp. 51–124, 2012.

[9] D. M. Sykora and P. de Groot, in *Proceedings of Optical Manufacturing and Testing IX*, Edited by J. H. Burge, O. W. Fahnle, and R. Williamson, Eds., Article ID 812610, Bellingham, WA, USA, 2011.

[10] Zygo, "Zygo interferometer," 2017, http://www.zygo.com/?/met/interferometers/dynafiz/.

[11] N. Bobroff, "Residual errors in laser interferometry from air turbulence and nonlinearity," *Applied Optics*, vol. 26, no. 13, p. 2676, 1987.

[12] J. Zhang, Z. H. Lu, and L. J. Wang, "Precision refractive index measurements of air, N_2, O_2, Ar, and CO_2 with a frequency comb," *Applied Optics*, vol. 47, no. 17, p. 3143, 2008.

[13] M. Assarar, A. El Mahi, and J.-M. Berthelot, "Evaluation of the dynamic properties of PVC foams under flexural vibrations," *Composite Structures*, vol. 94, no. 6, pp. 1919–1931, 2012.

[14] K. Kanny, H. Mahfuz, L. A. Carlsson, T. Thomas, and S. Jeelani, "Dynamic mechanical analyses and flexural fatigue of PVC foams," *Composite Structures*, vol. 58, no. 2, pp. 175–183, 2002.

[15] ANSYS Inc., Mechanical APDL Theory Reference Manual, Release 16.2.

[16] C. R. Farrar and K. Worden, *Structural Health Monitoring: A Machine Learning Perspective*, John Wiley & Sons, Chichester, UK, 2012.

[17] S. T. Gulati and M. J. Edwards, *ULE-Zero Expansion, Low Density, and Dimensionally Stable Material for Lightweight Optical Systems*, International Society for Optics and Photonics, Bellingham, WA, USA, 2017.

[18] X. Chen, W. Wu, X. Fu, and Y. Xu, in *Proceedings of 5th International Symposium on Advanced Optical Manufacturing and Testing Technologies: Large Mirrors and Telescopes*, vol. 7654, Edited by W. Jiang, M. K. Cho, and F. Wu, Eds., Article ID 76541K, Dalian, China, April 2010.

[19] R. Ceravolo, G. Pistone, L. Zanotti Fragonara, S. Massetto, and G. Abbiati, "Vibration-based monitoring and diagnosis of cultural heritage: a methodological discussion in three examples," *International Journal of Architectural Heritage*, vol. 10, no. 4, pp. 375–395, 2016.

[20] A. Agneni, L. B. Crema, and G. Coppotelli, "Modal parameters directly estimated from power spectral densities or correlation functions in output-only analysis," *Experimental Techniques*, vol. 40, no. 1, pp. 311–321, 2016.

[21] E. J. Hudson and P. Reynolds, "Design and construction of a reconfigurable pedestrian structure," *Experimental Techniques*, vol. 41, no. 2, pp. 203–214, 2017.

[22] K. Hacıefendioğlu and E. E. Maraş, "Photogrammetry in documentation and ambient vibration test of historical masonry minarets," *Experimental Techniques*, vol. 40, no. 6, pp. 1527–1537, 2016.

[23] M. Meo and G. Zumpano, "On the optimal sensor placement techniques for a bridge structure," *Engineering Structures*, vol. 27, no. 10, pp. 1488–1497, 2005.

[24] B. Peeters, H. Van der Auweraer, P. Guillaume, and J. Leuridan, "The PolyMAX frequency-domain method: a new standard for modal parameter estimation?," *Shock and Vibration*, vol. 11, no. 3-4, pp. 395–409, 2004.

[25] R. J. J. Allemang, "The modal assurance criterion–twenty years of use and abuse," *Journal of Sound and Vibration*, vol. 37, no. 8, pp. 14–21, 2003.

[26] G. Boscato, S. Russo, R. Ceravolo, and L. Zanotti Fragonara, "Global sensitivity-based model updating for heritage

structures," *Computer-Aided Civil and Infrastructure Engineering*, vol. 30, no. 8, pp. 620–635, 2015.

[27] F. Shabbir and P. Omenzetter, "Model updating using genetic algorithms with sequential niche technique," *Engineering Structures*, vol. 120, pp. 166–182, 2016.

[28] M. I. Friswell and J. E. Mottershead, *Finite Element Model Updating in Structural Dynamics*, Springer Science & Business Media, Berlin, Germany, 1995.

[29] D. J. Ewins, *Modal Testing: Theory, Practice and Application*, Research Studies Press Ltd., Baldock, UK, 2nd edition, 2000.

[30] W. Liu and D. J. Ewins, "Transmissibility properties of MDOF systems," in *Proceedings of 16th International Modal Analysis Conference*, vol. 2, pp. 847–854, Santa Barabara, CA, USA, February 1998.

[31] N. M. M. Maia, J. M. M. Silva, and A. M. R. Ribeiro, "The transmissibility concept in multi-degree-of-freedom systems," *Mechanical Systems and Signal Processing*, vol. 15, no. 1, pp. 129–137, 2001.